Incorporation of matter into characteristic numerical relativity

Nigel T. Bishop,[1] Roberto Gómez,[2] Luis Lehner,[2,3] Manoj Maharaj,[4] and Jeffrey Winicour[2]
[1]*Department of Mathematics, Applied Mathematics and Astronomy, University of South Africa, P.O. Box 392, Pretoria 0003, South Africa*
[2]*Department of Physics and Astronomy, University of Pittsburgh, Pittsburgh, Pennsylvania 15260*
[3]*Center for Relativity, The University of Texas at Austin, Austin, Texas 78712*
[4]*Department of Mathematics and Applied Mathematics, University of Durban-Westville, Durban 4000, South Africa*
(Received 8 December 1998; published 3 June 1999)

A code that implements Einstein's equations in the characteristic formulation in 3D has been developed and thoroughly tested for the vacuum case. Here, we describe how to incorporate matter, in the form of a perfect fluid, into the code. The extended code has been written and validated in a number of cases where shocks do not form. It is stable and capable of contributing towards an understanding of a number of problems in black hole astrophysics. [S0556-2821(99)00614-1]

PACS number(s): 04.25.Dm, 04.30.Db

I. INTRODUCTION

A code based on the characteristic formulation of general relativity (GR) has been developed for the general 3D problem [1]. The code computes the gravitational field of the full Einstein equations for a vacuum spacetime between some inner timelike world tube Γ and future null infinity. The code has been tested with the inner world tube Γ being the past horizon of a Schwarzschild black hole, with incoming gravitational radiation scattered off the black hole. The tests have included both linear and highly nonlinear regimes, and show the robustness of the characteristic formulation in the study of radiative problems. Here we consider whether there are real astrophysical problems to which the characteristic code alone could be applied.

Astrophysical problems that can be tackled by the code require the existence of a natural inner world tube Γ on which boundary data are known. This could be the past horizon in the inner region of a known stationary black hole of Kerr-Newman type, with the matter evolving in the outer region. However, boundary and initial data for the characteristic formulation are presently known only in the Schwarzschild case and in some multi-hole vacuum spacetimes [2]. When matter is incorporated into the code the range of possible astrophysical applications is greatly extended. In principle it is then possible to compute, in full nonlinear general relativity, the gravitational field and matter flow of a black hole accreting dust and gas, and of a black hole capturing polytropic or more realistic approximations to neutron stars. This paper does not solve any of these important astrophysical problems, but rather it lays the groundwork for doing so, by demonstrating the stability and convergence of a general 3D characteristic code for matter plus gravity.

The goal of this work is to establish *stability* of a characteristic evolution combining matter and gravity. Our matter code itself is rather simplistic and would not be expected to yield accurate results in cases of shock formation. The results of this paper are intended to show the feasibility of a characteristic gravity and matter evolution, which ultimately would incorporate a hydrodynamic code capable of an accurate handling of shocks.

The most popular approach to numerical relativity has been based on a Cauchy, rather than a characteristic, formalism, and a number of such codes incorporate hydrodynamics [3]. Yet the type of problem envisaged in this paper—a black hole capturing some form of star—has not been solved by these codes. The reason is that current 3D Cauchy gravity codes incorporating dynamic black holes have instability problems, and usually can be run for only a couple of light-crossing times. The great advantage of characteristic numerical relativity is that it has been demonstrated to be long-term stable [1], even in the presence of a dynamic event horizon [4]. Additionally, it has recently been shown that a high resolution shock-capturing version of the fluid equations can be successfully implemented in the characteristic formulation under the assumption of spherical symmetry [5]. The robustness of the numerical implementation of the characteristic formulation and the promising results obtained in [5] indicate that a characteristic evolution is a prime candidate for computing a variety of astrophysical processes.

The incorporation of matter into a characteristic code has been discussed previously. An axisymmetric code with matter has been used to consider a problem in cosmology [6]. Spherically symmetric matter codes, which include Cauchy-characteristic matching, have been reported [7,8]; see also [9]. In contrast, the present work has no symmetry requirement.

The paper restricts attention to matter in the form of a perfect fluid, by which we mean that the pressure p is a function *only* of the density ρ. In Sec. II we summarize known results, and introduce our notation, for the characteristic formalism and perfect fluid evolution. Next, in Sec. III we derive the fluid evolution equations in our characteristic coordinates; we also find the additional terms (compared to the vacuum case) that appear in Einstein's equations. Section IV describes details of the numerical implementation of the fluid evolution equations (the additional terms in Einstein's equations are straightforward to code). The resulting matter plus gravity code has been run on a variety of test problems, and the results are described in Sec. V. In all cases, the code is found to be stable and convergent. We end with a conclu-

sion (Sec. VI), and an appendix that contains expressions from Sec. III that are rather long.

II. FORMALISM

A. Null cone: Previous results

The formalism for the numerical evolution of Einstein's equations, in null cone coordinates, is well known [1,10] (see also [11–14]). Nevertheless, for the sake of completeness, we give here a summary of the formalism, including the necessary equations. We will use the notation and language of [1].

We use coordinates based upon a family of outgoing null hypersurfaces. We let u label these hypersurfaces, x^A ($A=2,3$), label the null rays and r be a surface area coordinate. In the resulting $x^\alpha=(u,r,x^A)$ coordinates, the metric takes the Bondi-Sachs form [14,15]

$$ds^2=-\left[e^{2\beta}\left(1+\frac{W}{r}\right)-r^2h_{AB}U^AU^B\right]\times du^2-2e^{2\beta}dudr-2r^2h_{AB}U^Bdudx^A+r^2h_{AB}dx^Adx^B, \tag{1}$$

where W is related to the more usual Bondi-Sachs variable V by $V=r+W$, and where $h^{AB}h_{BC}=\delta^A_C$ and $\det(h_{AB})=\det(q_{AB})$, with q_{AB} a unit sphere metric. In analyzing Einstein's equations, we also use the intermediate variable

$$Q_A=r^2e^{-2\beta}h_{AB}U^B_{,r}. \tag{2}$$

We work in stereographic coordinates $x^A=(q,p)$ for which the unit sphere metric is

$$q_{AB}dx^Adx^B=\frac{4}{P^2}(dq^2+dp^2), \tag{3}$$

where

$$P=1+q^2+p^2. \tag{4}$$

We also introduce a complex dyad q_A defined by

$$q^A=\frac{P}{2}(1,i) \tag{5}$$

with $i=\sqrt{-1}$. For an arbitrary Bondi-Sachs metric, h_{AB} can then be represented by its dyad component

$$J=h_{AB}q^Aq^B/2, \tag{6}$$

with the spherically symmetric case characterized by $J=0$. The full nonlinear h_{AB} is uniquely determined by J, since the determinant condition implies that the remaining dyad component

$$K=h_{AB}q^A\overline{q^B}/2 \tag{7}$$

satisfies $1=K^2-J\overline{J}$. We also introduce spin-weighted fields

$$U=U^Aq_A, \quad Q=Q_Aq^A, \tag{8}$$

as well as the (complex differential) eth operators ð and $\bar{\text{ð}}$ (see [16] for full details).

The Einstein equations $G_{ab}=0$ decompose into hypersurface equations, evolution equations and conservation laws. Naturally, the equations will require additional terms to allow for the presence of matter, and the extended equations are given later in Sec. III B. Here we just note that the hypersurface equations form a hierarchical set for $\beta_{,r}$, $(r^2Q)_{,r}$, $U_{,r}$ and $W_{,r}$, and the evolution equation is an expression for $(rJ)_{,ur}$.

The remaining independent equations are the conservation conditions, but they will not be needed here.

The null cone problem is normally formulated in the region of spacetime between a timelike or null world tube Γ and $\mathcal{I}^+$, with initial data J given on the null cone $u=0$ in this domain. Boundary data for β, Q, U, W and J is also required on Γ. The metric variables used remain regular at $\mathcal{I}^+$, and we represent $\mathcal{I}^+$ on a finite grid by using a compactified radial coordinate $x=r/(1+r)$.

B. Perfect fluid: Previous results

The description of a perfect fluid is well understood (e.g. [17,18]). The stress-energy tensor is

$$T_{ab}=(\rho+p)v_av_b+pg_{ab} \tag{9}$$

where ρ is the density, p is the pressure, v_a is the 4-velocity and g_{ab} is the metric. In the cases considered here, the pressure depends *only* on the density, i.e.

$$p=p(\rho). \tag{10}$$

The matter evolution equations follow from the conservation law $T^{ab}{}_{;b}=0$, and are

$$\rho_{,a}v^a+(\rho+p)v^a_{;a}=0, \quad (\rho+p)v_{a;b}v^b+(\delta^b_a+v_av^b)p_{,b}=0, \tag{11}$$

which may be rewritten as

$$\rho_{,a}v_bg^{ab}+(\rho+p)(v_{a,b}-\Gamma^c_{ab}v_c)g^{ab}=0 \tag{12}$$

$$M_a\equiv(\rho+p)(v_{a,b}-\Gamma^c_{ab}v_c)v_dg^{bd}+p_{,a}+v_av_cp_{,b}g^{bc}=0. \tag{13}$$

The numerical implementation of the fluid equations coupled to GR has been investigated primarily within the 3+1 or Cauchy framework. In this formulation, the spacetime is foliated by a sequence of spacelike surfaces, initial data are given on an initial surface and the evolution equations are used to compute the future. The numerical investigation of the ''GR-hydro'' problem started in the early 1970s by Wilson [19] and since then it has received considerable attention. The difficulty of modeling these equations has spurred the development of sophisticated techniques to deal with the diverse idiosyncracies of the problem. Thus, artificial viscosity techniques, total variation diminishing flux limiters,

shock-capturing schemes, etc., are actively employed to aid in the numerical modeling; refer to [3] for a recent review.

Another problem one faces when attempting a numerical simulation in the 3+1 formalism is that an artificial ''outer boundary'' has to be included at some radius in order to deal with a finite grid. This introduces spurious reflections that spoil long term evolutions. In the characteristic formulation, on the other hand, one can use Penrose's compactification techniques to include infinity in the numerical grid. Additionally, being able to access null infinity allows one to obtain physical quantities, such as the radiation given off by the system and the total mass, unambiguously. There is not as much experience with the GR-hydro problem in the characteristic formulation, but the results obtained in [5] and this paper indicate that the characteristic formulation of GR will be a valuable tool in the study of a variety of astrophysical problems.

III. PERFECT FLUID IN THE NULL CONE FORMALISM

A. Perfect fluid equations

In order to proceed further we represent the angular part of the 4-velocity by means of the complex quantity

$$V_{ang}=q^A v_A=\frac{P}{2}(v_2+iv_3), \tag{14}$$

where the *ang* suffix is introduced to avoid confusion with the Bondi-Sachs metric variable V. The matter evolution equations are then:

(i) Equation (12).

(ii) Equation (13) in the form

$$M_1=0, \quad q^A M_A=0. \tag{15}$$

We also introduce the notation

$$p_\rho=\frac{1}{p+\rho}\frac{dp}{d\rho} \tag{16}$$

and then write

$$p_{,a}=p_\rho(p+\rho)\rho_{,a}. \tag{17}$$

The result of doing this is that, in the matter evolution equations, there is no explicit division by $(p+\rho)$ (which could be zero). From a numerical point of view, it is possible to write the procedure for computing p_ρ so as to ensure its good behavior in the low density limit.

The matter evolution equations have been calculated using MAPLE; they are rather long and are given in the Appendix. The denominators are important in determining whether there may be singular behavior, and here we note that the form of the equations is

$$\rho_{,u}=\frac{1}{r^3(v_1)^2\left(\frac{dp}{d\rho}-1\right)}F_\rho \tag{18}$$

$$v_{1,u}=\frac{1}{r^3 v_1\left(\frac{dp}{d\rho}-1\right)}F_1 \tag{19}$$

$$V_{ang,u}=\frac{1}{r^2 v_1}F_V. \tag{20}$$

Formally, Eqs. (18) and (19) could be singular if $dp/d\rho$ were to be 1, but this would correspond physically to the velocity of sound being equal to that of light. We do not concern ourselves with those cases at the moment and defer its treatment for a later work. Also, Eqs. (18), (19) and (20) could be singular if v_1 were to be zero; yet, starting from $-1=v_a v_b g^{ab}$,

$$v_1 e^{-2\beta}\left(\frac{V}{r}v_1-2v_0-2U^A v_A\right)\leqslant -1, \tag{21}$$

which can never be satisfied if $v_1=0$. Thus, from an analytic point of view, Eqs. (18), (19) and (20) form a well-behaved set of evolution equations.

Finally, again using the condition $-1=g^{ab}v_a v_b$, we obtain an expression for the remaining velocity component v_0:

$$v_0=\frac{e^{2\beta}(2KV_{ang}\bar{V}_{ang}-J\bar{V}^2_{ang}-\bar{J}V^2_{ang}+2r^2)+2rv_1(Vv_1-rU\bar{V}_{ang}-r\bar{U}V_{ang})}{4v_1 r^2}. \tag{22}$$

B. Einstein's equations

The introduction of matter also amends Einstein's equations. We write the equations as

$$R_{ab}=8\pi\left(T_{ab}-\frac{1}{2}g_{ab}T\right), \tag{23}$$

and note that

$$T=-(\rho+p)+4p=3p-\rho. \tag{24}$$

Thus Einstein's equations for a perfect fluid are

$$R_{ab}=8\pi(\rho+p)v_a v_b+g_{ab}\left(p-\frac{3p-\rho}{2}\right)$$
$$=8\pi\left((\rho+p)v_a v_b+g_{ab}\frac{\rho-p}{2}\right). \tag{25}$$

In the expressions below, N_β, N_U, N_Q, N_W and N_J represent the nonlinear aspherical terms (in a sense specified in

[10]). These quantities are quite long and are not repeated here since they have been given explicitly in [1]. Using MAPLE we have confirmed that

(i) R_{11} in Eq. (25) leads to

$$\beta_{,r}=N_\beta+2\pi r(\rho+p)(v_1)^2. \tag{26}$$

(ii) $R_{1A}q^A$ in Eq. (25) leads to

$$(r^2Q)_{,r}=-r^2(\bar{\eth}J+\eth K)_{,r}+2r^4\eth(r^{-2}\beta)_{,r} +N_Q+16\pi r^2(\rho+p)v_1V_{ang}. \tag{27}$$

(iii) The equation for U is a definition, and so the presence of matter does not change it:

$$U_{,r}=\frac{e^{2\beta}}{r^2}(KQ-J\overline{Q}). \tag{28}$$

(iv) $R_{AB}h^{AB}$ in Eq. (25) leads to

$$W_{,r}=\frac{1}{2}e^{2\beta}\mathcal{R}-1-e^{\beta}\eth\bar{\eth}e^{\beta}+\frac{1}{4}r^{-2}(r^4(\eth\overline{U}+\bar{\eth}U))_{,r} +N_W-4\pi e^{2\beta}\Big[(\rho+p)\Big(KV_{ang}\overline{V}_{ang} -\frac{1}{2}(J\overline{V}^2_{ang}+\overline{J}V^2_{ang})\Big)+(\rho-p)r^2\Big], \tag{29}$$

where

$$\mathcal{R}=2K-\eth\bar{\eth}K+\frac{1}{2}(\bar{\eth}^2J+\eth^2\overline{J})+\frac{1}{4K}(\bar{\eth}\overline{J}\eth J-\bar{\eth}J\eth\overline{J}). \tag{30}$$

(v) $R_{AB}q^Aq^B$ in Eq. (25) leads to

$$2(rJ)_{,ur}-(r^{-1}V(rJ)_{,r})_{,r}=-r^{-1}(r^2\eth U)_{,r}+2r^{-1}e^{\beta}\eth^2e^{\beta}-(r^{-1}W)_{,r}J+N_J +\frac{4e^{2\beta}\pi}{r}[V^2_{ang}(\rho+p)+r^2J(\rho-p)]. \tag{31}$$

C. Summary

The data required on the initial null cone are:

$$J,\ \rho,\ v_1,\ V_{ang}, \tag{32}$$

and these constitute the set of evolution variables. The auxiliary variables may then be determined on the initial null cone, and they are found in the following order: p from the equation of state, β from Eq. (26), Q from Eq. (27), U from Eq. (28), W from Eq. (29), and v_0 from Eq. (22). The evolution equations (31), (18), (19) and (20) may now be used to find J, ρ, v_1 and V_{ang} (in that order) on the ''next'' null cone.

In order to have a properly specified problem, we will also need boundary data on the timelike world tube Γ. For the gravitational variables this data is β, Q, U, W and J, and for the matter variables we will need ρ, v_1 and V_{ang}.

IV. NUMERICAL IMPLEMENTATION

We constructed a set of algorithms to solve Eqs. (26)–(31). In discretizing the equations we follow closely the strategy developed for the vacuum case [1]. We introduce a compactified radial coordinate $x=r/(1+r)$ and define the numerical grid with coordinates $(u^n,x_i,q_j,p_k)=(n\Delta u,1/2+(i-1)\Delta x,-1+(j-3)\Delta q,-1+(j-3)\Delta p)$ [where $2\Delta x=1/(N_x-1)$, and $\Delta q=\Delta p=2/(N_\xi-1)$]. Using finite differences to discretize the equations, we center the derivatives at $(n+1/2,i-1/2,j,k)$.

The evolution equation is treated as in [1] where the right hand side is modified to include the matter terms. Thus, the matter variables at $(n+1/2,i-1/2)$ are evaluated by taking the average between the values at $(n+1,i-1)$ and (n,i), while the radial derivatives are obtained from the average of the corresponding values at $(n+1,i-3/2)$ and $(n,i+1/2)$.

Next, we proceed to integrate the evolution equation of the matter variables by a simple iterative method which results in a second order in space, second order in time scheme, as follows. First, note that the matter equations can be schematically written as

$$g_{,u}=F; \tag{33}$$

then, a direct second order discretization is obtained by

$$g_i^{n+1}=g_i^n+\Delta uF_i^{n+1/2}. \tag{34}$$

Note that F depends on the matter fields; thus without having at hand the value of g_i^{n+1}, F cannot be directly evaluated at the midpoint. However, the value of $F_i^{n+1/2}$ can indeed be obtained by a straightforward iteration. In the first step we set $F_i^{n+1/2}=F_i^n$ and use it to evaluate the right hand side of Eq. (34); then, the obtained approximation to g_i^{n+1} is used to obtain a better approximation to $F_i^{n+1/2}$ and so on. This procedure is repeated a sufficient number of times to ensure second order convergence of the algorithm.

However, the above procedure must be carefully applied at the horizon, where divergent fields can spoil the numerical modeling of the problem. The properties of our coordinates are easy to understand in the vaccum case, in which the metric quantities satisfy $\beta=U=J=0$, $W=-2M$, and the metric (1) is the Schwarzschild metric in outgoing

Eddington-Finkelstein form. In the Kruskal diagram for these coordinates, the past horizon is at $r=2M$, u finite, and the future horizon, at $u=\infty$. There is a coordinate singularity where the past horizon meets the future horizon at $r=2M$, $u=\infty$. In the presence of infalling matter, this inevitably leads to a divergence as the inner portion approaches the black hole. In the formulation used here, the singularity manifests itself as a divergence in the velocity component v_1. Because the grid is based on the r coordinate, the numerical method is sensitive to the details of treating the region near $r=2M$.

In particular, this applies to the start-up procedure at the inner boundary of the computational domain on the past horizon. The following method was found to be stable. The matter fields at the first point outside $r=2M$ are evolved by employing a *one sided* differences to evaluate radial derivatives in F. Further, the derivatives are evaluated only at the lower time level and are centered at $(n,i+1/2)$ rather than at $(n+1/2,i-1/2)$. Thus the scheme is only first order accurate in both Δu and Δx—unfortunately all second order schemes that we investigated were unstable. The issue of the global accuracy of our numerical method is now discussed. At the analytic level, matter never reaches the past horizon, but numerical error travels faster than light, and matter, in the form of second order discretization error, may reach the past horizon. The error introduced by applying a first order method to second order error remains second order. Therefore, in the limit as $\Delta x\rightarrow 0$, the global accuracy of the scheme should be second order. However, in practice (due to finite computer resources) Δx cannot be made smaller than about 10^{-2}. The global accuracy of the scheme will be reduced once there is a non-zero analytic matter field at the second grid point from $r=2M$; for $\Delta x=10^{-2}$ this point is located at $r=2.12M$, and analytic infalling matter reaches this point at some finite time. The possible improvement of the boundary algorithm is deferred to future work.

Finally, the hypersurface equations are discretized as in [1], where the right hand sides now include the matter variables evaluated at $(n+1,i-1/2)$ [which is straightforward having the matter fields values at $(n+1,i)$ obtained in the previous step].

V. TESTS AND RESULTS

We test the code by considering an initial localized distribution of matter around a Schwarzschild black hole with mass taken to be $M=1$. The gravitational initial data are taken as

$$J(u=0,r,x^A)=0. \tag{35}$$

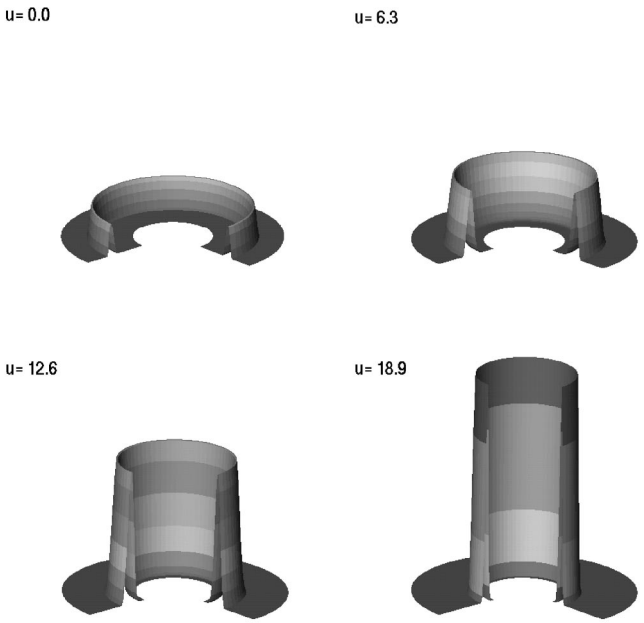

FIG. 1. Density profiles vs time. The figure shows 4 different snapshots of ρ at the equator. The inner part ''hole'' in the pictures corresponds to the black hole $r=2m$ radius while the outer part corresponds to $r=\infty$. The collapse of matter onto the black hole can be clearly seen. The plots are for the case $\lambda=10^{-9}$ and $p\neq 0$.

For a non-spherical initial distribution of matter, this condition is in a sense unphysical in that it will introduce spurious incoming gravitational radiation [20,21]; nevertheless, it is simple and is suitable for code testing. The gravitational boundary data on the world tube Γ, which we take to be the past horizon of the black hole at $r=2$, are [1]

$$\beta=0, \quad Q=0, \quad U=0, \quad W=-2, \quad J=0. \tag{36}$$

The initial data for the tests include two different distributions of the matter:

(i) Spherical shell that falls radially towards the black hole.

(ii) Localized blob of matter falling radially towards the black hole.

The tests are performed for two different equations of state:

(i) Dust $(p=0)$.

(ii) Fluid with $p\propto\rho^{1.4}$.

A. Initial and boundary data for the matter

We assume

$$\rho(u=0,r,x^A)=\begin{cases}\lambda\exp\left(-\dfrac{R_b-R_a}{2(r-R_a)}\right)\exp\left(-\dfrac{R_b-R_a}{2(R_b-r)}\right)G(x^A) & \text{if } r\in[R_a,R_b],\\ 0 & \text{otherwise.}\end{cases} \tag{37}$$

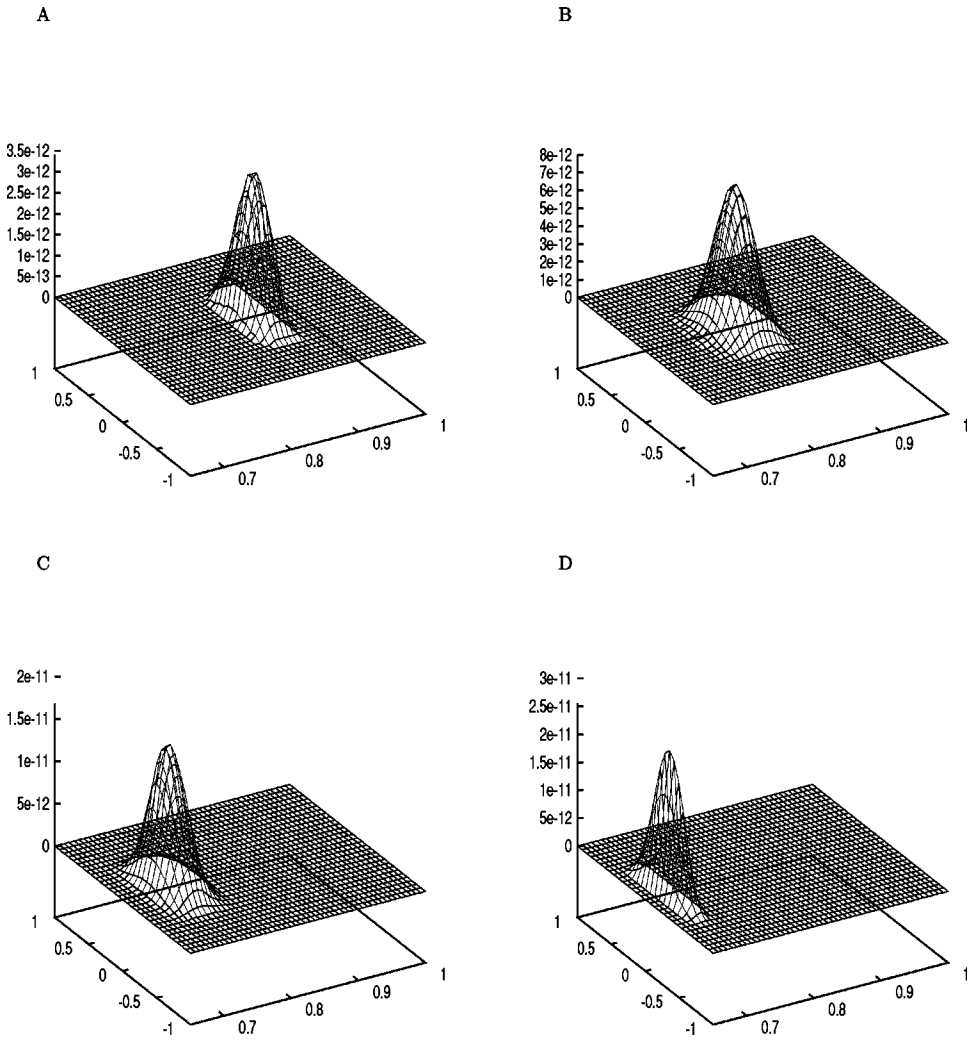

FIG. 2. Density profiles vs time for the localized ''blob'' of matter at times $u=0$ (A), $u=7.2$ (B), $u=14.3$ (C) and $u=21.5$ (D). The value of initial amplitude parameter for this case is $\lambda=10^{-9}$, and $p\neq 0$. The figure shows 4 different snapshots of ρ at $y=0$ (on the northern hemisphere) as a function of the compactified radial coordinate ($x=2/3$ being the black hole radius and $x=1$ corresponding to null infinity). The pulse collapses onto the black hole, remaining localized.

If $G(x^A)=1$, ρ describes a spherical shell of matter between $r=R_a$ and $r=R_b$, and centered about $r=0$. We also consider the case with G defined as a localized Gaussian-type function:

$$G(x^A)=\begin{cases}(q^2+p^2-\mu)^4 & \text{if } q^2+p^2\leqslant\mu,\\ 0 & \text{otherwise,}\end{cases} \tag{38}$$

which we use to describe an initial ''blob'' of matter. To provide initial data for the velocity field, we set $V_{ang}=0$ and

$$v_{rn}(u=0,r,x^A)=-(\sqrt{1+E}+\sqrt{E+2/r})(1-2/r) \tag{39}$$

where v_{rn} is v_1 renormalized to be well behaved on the event horizon $r=2$ [explicitly $v_{rn}=v_1(1-2/r)^2$]. E represents the energy at infinity of a unit mass particle, in the sense that at infinity $|v^1|^2=E$; note that $E>-1$. In the tests described below we take

(i) $R_a=4$ and $R_b=7$.

(ii) λ varying between 10^{-5} and 10^{-13}.

(iii) $G(x^A)=1$ (spherical shell) or $G(x^A)$ given by Eq. (38) with $\mu=0.4$ (blob of matter with center at one of the poles whose density goes to zero at about $\theta=44°$).

(iv) $E=2.25$.

Analytically, the matter never reaches $r=2$, but in practice, due to numerical diffusion, boundary conditions are still needed there; we impose

$$\rho=0, \quad V_{ang}=0, \quad v_{rn}=0. \tag{40}$$

B. Equation of state

For dust, the equation of state is $p=0$. We also investigate how the code copes with nonzero pressure, and set up a test case with the density defined as above (with $\lambda=10^{-9}$), and with the equation of state

$$p=\omega\rho^{1.4}, \tag{41}$$

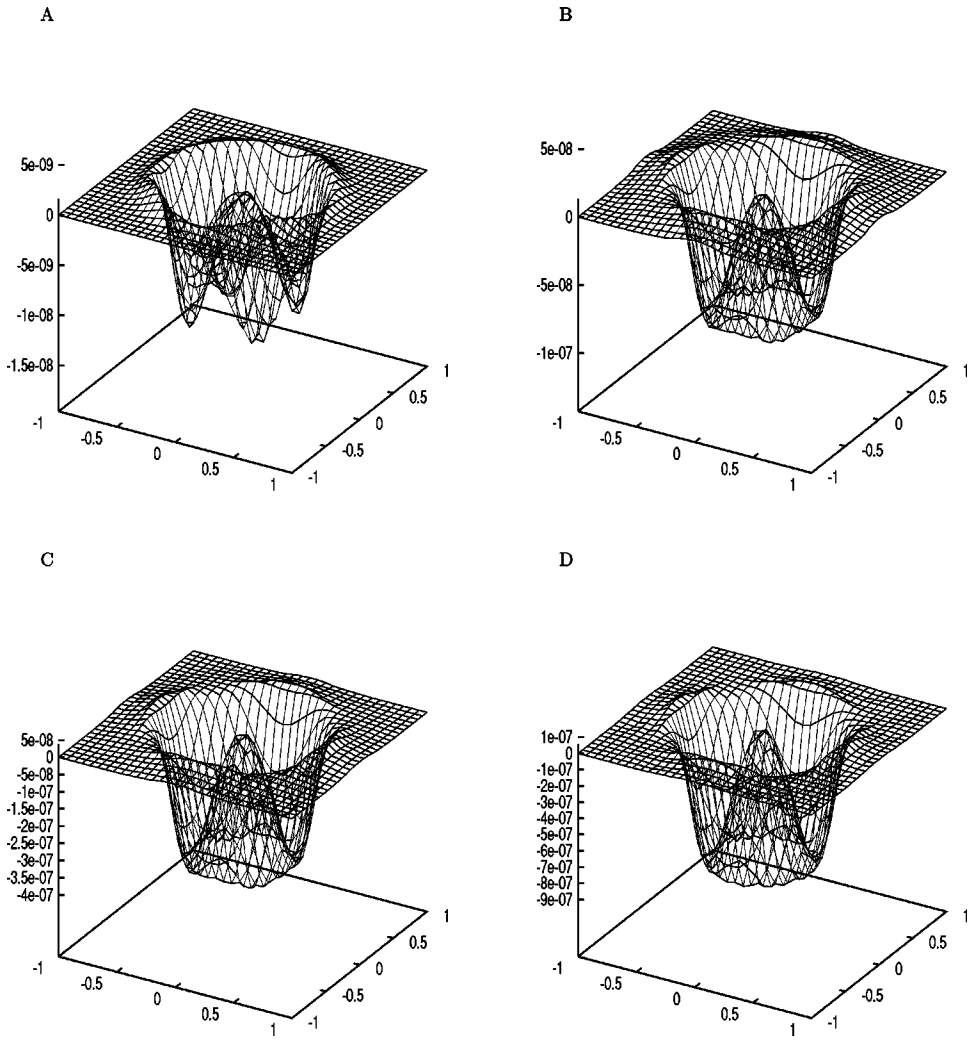

FIG. 3. The ''plus'' component of the news on the northern hemisphere for the case $\lambda = 10^{-9}$ and $p \neq 0$ at times $u = 0$ (A), $u = 7.2$ (B), $u = 14.3$ (C) and $u = 21.5$ (D).

with $\omega = 10^{-11}$. Further, in order to keep p_ρ [Eq. (16)] well behaved for small ρ, we set $p = 0$ whenever $\rho < \rho_{max} 10^{-5}$, where ρ_{max} is the maximum value of ρ at $u = 0$. Although the magnitude of the pressure is small, and our implementation of the fluid equations is rather simple, it is encouraging to see that there is no evidence of any pressure-related instability. More realistic initial data and equations of state could induce shocks that would require a sophisticated treatment of the matter equations. We defer this to future work.

C. Physical interpretation of the initial data

It is useful to clarify the issue of units. We are using geometric units in which $G = c = 1$, and everything is given in terms of a unit of length, which is the distance corresponding to a unit change in the radial coordinate r. Fixing the event horizon at $r = 2$, the geometric unit of length is the mass of the black hole M.

The range of initial data sets that are used can be described by considering the ratio of the characteristic length associated with the density to M. Modulo a constant of order unity, this ratio is $R_\rho = (\sqrt{\lambda} M)^{-1}$, and in the tests the parameter R_ρ varies between 3.16×10^2 to 3.16×10^6. A similar analysis can be made on the pressure and we find $R_p = \omega^{1.25}/M$, in the tests $R_p = 0$ and R_ρ in the range just described, or $R_p = 1.78 \times 10^{-14}$ and $R_\rho = 3.16 \times 10^4$.

Conversion to SI units needs the value of M in meters. We write

$$M = r_0 \quad [\mathrm{m}], \tag{42}$$

where, for example, a $10 M_\odot$ black hole has $r_0 = 14766$ [m]. Using the notation that quantities in geometric units will be denoted without suffix, and those in SI units will have the suffix S, the conversions for speed v, mass m, density ρ and pressure p are

$$v \times 2.998 \times 10^8 = v_S \ [\mathrm{m/s}]$$

$$m \times 1.347 r_0 \times 10^{27} = m_S \ [\mathrm{kg}]$$

$$\rho \times \frac{1.347 \times 10^{27}}{r_0^2} = \rho_S \ [\mathrm{kg/m^3}]$$

$$p \times \frac{1.210 \times 10^{44}}{r_0^2} = p_S \ \text{[Pa]}. \tag{43}$$

We now use these conversions to determine, in SI units, the various parameters describing the initial data specified above, when the mass of the black hole is $10M_\odot$ and $\lambda = 10^{-9}$:

(i) *Spherical shell:* $\rho_S = 8.34 \times 10^8\ kg/m^3$, $v = 0.90c$, $p_S = 0$ or $p_S = 8.47 \times 10^{10}\ Pa$, $m = 3.37 \times 10^{-6} M_\odot$,

(iii) *Localized pulse:* $\rho_S = 2.14 \times 10^7\ kg/m^3$, $v = 0.90c$, $p_S = 0$ or $p_S = 5.01 \times 10^8\ Pa$, $m = 6.11 \times 10^{-9} M_\odot$,

where v is the proper inward radial velocity, m is the mass of the shell or pulse, and the values of ρ_S, p_S and v are given at the point of maximum density at $u = 0$. For $\lambda \neq 10^{-9}$, ρ_S and m scale linearly in λ, p_S scales as $\lambda^{1.4}$, and v is unchanged. The scaling with r_0, which represents the mass of the black hole, is given by Eq. (43).

D. Spherical collapse

The first test was the collapse of a spherical shell onto a black hole. We set the black hole mass $= 1$, the inner boundary of the shell at $R_a = 4$ and the outer boundary at $R_b = 7$. The resulting spacetime is spherically symmetric. This symmetry provides checks on the accuracy of the numerical evolution since it implies that no gravitational radiation should be emitted and that J must vanish everywhere.

We confirmed this behavior by monitoring the L_2 norms of J and the news function for different initial amplitudes $\lambda = 10^{-(2n+5)}$ (with $n = 0, \ldots, 4$) over time (with $u \in [0,2]$). At any given time, the value of $||J||_2$ and each polarization mode converges to zero as the discretization is refined. The matter collapses onto the black hole and the run proceeds smoothly. Figure 1 shows the evolution of ρ for the case with pressure.

Additionally, it is straightforward to calculate analytically the total Bondi mass of the system; using MAPLE we found that (for $p = 0$, $\lambda = 10^{-6}$) $M_T = 1.0007395$. By increasing the resolution, we checked that this value is approached, to second order accuracy, by the value computed from the code; the test was performed at both $u = 0$ and $u = 2$. For instance, with a grid of $N_x = 165$ and $N_\xi = 65$, the value obtained for the mass at $u = 2$ is $M_T = 1.0007408$, which agrees quite well with the expected value.

E. Black-hole–matter ball collision

To study the collision of a dustball–black-hole system we again set the black hole mass $M = 1$ and the inner and outer radii of the blob with $R_a = 4$ and $R_b = 7$; finally, the localization on the sphere is set by choosing $\mu = 0.4$. This configuration describes a ball of dust with center at one of the poles that goes to zero at about $\theta = 44°$ with compact support in [4,7] in the radial direction. Note that in this case, although we initially set $V_{ang} = 0$, the self-gravitational field of the dustball induces a non-zero V_{ang} towards the pole. Figure 2 displays the evolution of ρ for the case with pressure ($\lambda = 10^{-9}$). Again, the evolution proceeds smoothly as the ''blob'' of matter collapses onto the black hole and the plus polarization mode of the news is obtained at null infinity (see Fig. 3).

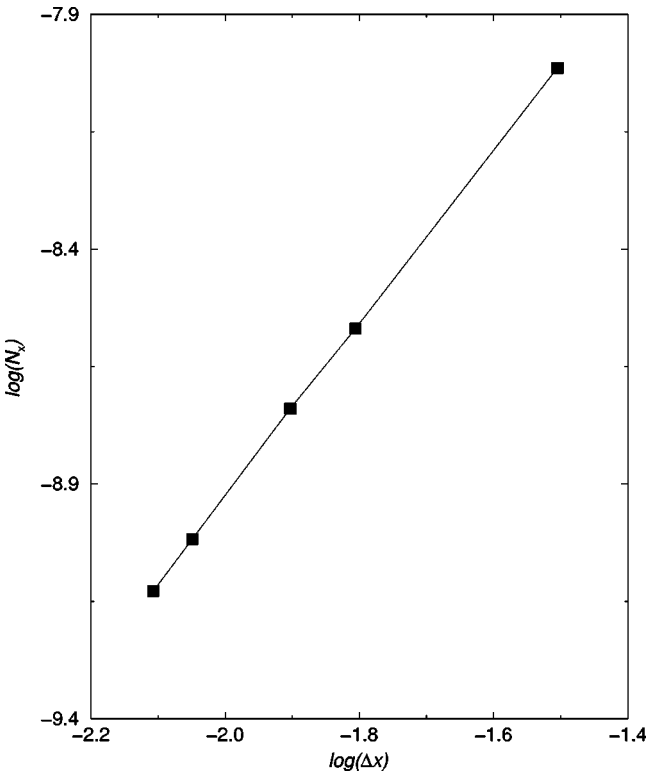

FIG. 4. Convergence of the *cross* polarization mode in an axisymmetric spacetime. The figure shows the logarithm of $N_\times(u = 0.15)$ vs the logarithm of the discretization size. The slope of 1.9 is in good agreement with second order convergence. The plot is for the case $\lambda = 10^{-9}$ and $p \neq 0$.

Although an analytic solution to this problem is unknown, one can check consistency of the obtained simulation by observing that the *cross* polarization mode ($\mathcal{N}_\times$) must vanish (since the problem is still axisymmetric). We confirmed this behavior, by increasing the number of grid points and plotting the logarithm of the L_∞ norm of $\mathcal{N}_\times$ (at $u = 0.15$) vs discretization size and observing its convergence to zero. As shown in Fig. 4 the slope of 1.9 is in agreement with second order convergence. The convergence test was performed with $\lambda = 10^{-9}$ and with non-zero pressure. We should add, however, that at later times ($u \geqslant 10$), the convergence rate is reduced to about 1.5. This is expected because of the non-centered scheme used at the black hole boundary (see Sec. IV).

Another check made was that the path of the peak density should be a geodesic of the background spacetime. This was indeed found to be the case. For example, using MAPLE we found that at $u = 2$, r should be 4.9169, and numerically we found, for the case $\lambda = 10^{-7}$ and non-zero pressure, that $r = 4.9180$ (for a grid with $N_x = 85$ and $N_\xi = 65$).

VI. CONCLUSION

In this paper, we have incorporated matter, in the form of a perfect fluid, into the characteristic code for the Einstein

field equations: we have found explicit forms for the various evolution and field equations, we have shown how these equations are discretized, and we have carried out a number of tests on the resulting code. The code is stable and convergent, and its validation has included the following tests.

(i) The peak of the matter ''blob'' follows a geodesic of the background spacetime.

(ii) The code is not written with any symmetries, yet symmetric initial data lead to the appropriate part of the gravitational radiation vanishing.

(iii) In the spherically symmetric case, the mass of the system, as calculated by the code, is conserved and agrees with the initial mass calculated analytically.

Taken together, and also with earlier validations of the pure gravity code [1], these tests provide substantial evidence that the code is correct in a regime free of shocks. The geodesic test provides evidence that the matter flow is correct, and the mass test shows that mass is being conserved during radial motion. Gravitational radiation is generated by angular asymmetries and motion, and the symmetry test shows that any error in the angular dependence of the matter variables would have to be carefully contrived so as to preserve the symmetries.

This paper has not computed a solution to any real problem in astrophysics. Nevertheless, we have shown that the present code is capable of modeling a variety of situations where matter is captured by a black hole, although our treatment of the hydrodynamics would need to be amended in order to be able to handle shock waves. Even so, the present code should be able to contribute towards an understanding of a number of problems in black hole astrophysics.

ACKNOWLEDGMENTS

The authors thank Philippos Papadopoulos, Jose Font, Richard Matzner, Matthew Choptuik and Ed Seidel for helpful comments. This work has been supported by NSF PHY 9510895 and NSF INT 9515257 to the University of Pittsburgh, by NSF PHY 9800722 and NSF PHY 9800725 to the University of Texas at Austin and by the Binary Black Hole Grand Challenge Alliance, NSF PHY/ASC 9318152. Computer time was provided by the Pittsburgh Supercomputing Center and the San Diego Supercomputer Center. L.L. was partially supported by the Mellon Foundation through the University of Pittsburgh. N.T.B. and M.M. thank the Foundation for Research Development, South Africa, for financial support. N.T.B. thanks the University of Pittsburgh for hospitality. L.L. thanks the Universities of South Africa and of Durban-Westville for their hospitality.

APPENDIX

The evolution equations for the matter variables are given below; note that V_w is $1+W/r$:

$$
\begin{aligned}
V_{ang,u}=&\frac{p_\rho}{4v_1r^2}\{[2e^{2\beta}(\overline{\delta\rho})\overline{V}_{ang}^2+2e^{2\beta}V_{ang}(\delta\rho)\overline{V}_{ang}]K-4V_{ang}\rho_{,r}v_0r^2-2V_{ang}\rho_{,r}\overline{V}_{ang}Ur^2\\
&-4V_{ang}\rho_{,u}v_1r^2+4e^{2\beta}(\delta\rho)r^2-2e^{2\beta}(\delta\rho)V_{ang}^2\overline{J}-2V_{ang}v_1(\delta\rho)\overline{U}r^2-2V_{ang}v_1(\bar{\delta}\rho)Ur^2\\
&+4V_{ang}\rho_{,r}v_1V_wr^2-2V_{ang}^2\rho_{,r}\overline{U}r^2-2e^{2\beta}V_{ang}(\bar{\delta}\rho)\overline{V}_{ang}J\}\\
&+\frac{1}{4v_1r^2}\{4v_1r^2U(\delta\beta)\overline{V}_{ang}-e^{2\beta}(\delta J)\overline{V}_{ang}^2-e^{2\beta}(\delta\overline{J})V_{ang}^2+4v_1r^2\overline{U}(\delta\beta)V_{ang}\\
&-4V_{ang,r}v_0r^2+4V_wV_{ang,r}v_1r^2-2e^{2\beta}(\delta V_{ang})V_{ang}\overline{J}-2v_1r^2(\delta\overline{U})V_{ang}\\
&+[2e^{2\beta}(\delta V_{ang})\overline{V}_{ang}+2e^{2\beta}(\bar{\delta}V_{ang})V_{ang}]K-4V_wv_1^2r^2(\delta\beta)-2e^{2\beta}(\bar{\delta}V_{ang})\overline{V}_{ang}J+2e^{2\beta}JK(\delta\overline{J})V_{ang}\overline{V}_{ang}\\
&+2e^{2\beta}\overline{J}K(\delta J)V_{ang}\overline{V}_{ang}-2v_1U(\bar{\delta}V_{ang})r^2\\
&-2e^{2\beta}(\delta K)V_{ang}\overline{V}_{ang}+2v_1^2r^2(\delta V_w)-4e^{2\beta}\overline{J}J(\delta K)V_{ang}\overline{V}_{ang}-2V_{ang,r}U\overline{V}_{ang}r^2\\
&+8v_0v_1r^2(\delta\beta)-2v_1\overline{U}(\delta V_{ang})r^2-2r^2v_1(\delta U)\overline{V}_{ang}-2V_{ang,r}\overline{U}V_{ang}r^2\},
\end{aligned}
\tag{A1}
$$

$$
\rho_{,u}=-\frac{e^{2\beta}[F_ov_1-F_a(p+\rho)]}{v_1^2[p_\rho(p+\rho)-1]},\quad v_{1,u}=\frac{e^{2\beta}(-F_a+F_ov_1p_\rho)}{v_1[p_\rho(p+\rho)-1]},
\tag{A2}
$$

with F_o and F_a given by

$$
\begin{aligned}
F_o=&\frac{p+\rho}{4e^{2\beta}r^2}\{[-2(\eth K)\overline{V}_{ang}e^{2\beta}-2(\bar{\eth}K)V_{ang}e^{2\beta}]J\overline{J}-2(\eth\overline{J})V_{ang}e^{2\beta}+[(\eth J)\overline{V}_{ang}e^{2\beta}\\
&+(\bar{\eth}J)V_{ang}e^{2\beta}]K\overline{J}+[(\eth\overline{J})\overline{V}_{ang}e^{2\beta}+(\bar{\eth}\overline{J})V_{ang}e^{2\beta}]KJ\\
&+8v_1rV_w-4v_{0,r}r^2-2v_1r^2(\bar{\eth}U)+[-2(\eth V_{ang})e^{2\beta}-4(\eth\beta)V_{ang}e^{2\beta}]\overline{J}+4V_wv_{1,r}r^2\\
&-2(\bar{\eth}J)\overline{V}_{ang}e^{2\beta}+[-4(\bar{\eth}\beta)\overline{V}_{ang}e^{2\beta}-2(\bar{\eth}\overline{V}_{ang})e^{2\beta}]J\\
&+[2(\eth\overline{V}_{ang})e^{2\beta}+4(\bar{\eth}\beta)V_{ang}e^{2\beta}+4(\eth\beta)\overline{V}_{ang}e^{2\beta}+2(\bar{\eth}V_{ang})e^{2\beta}]K\\
&-2U\overline{V}_{ang,r}r^2-2\overline{U}V_{ang,r}r^2+4v_1r^2V_{w,r}-8v_0r-2r^2\overline{U}_{,r}V_{ang}-2U(\bar{\eth}v_1)r^2\\
&-4r\overline{U}V_{ang}-4rU\overline{V}_{ang}-2r^2U_{,r}\overline{V}_{ang}-2v_1r^2(\eth\overline{U})-2\overline{U}(\eth v_1)r^2\}\\
&+\frac{1}{4e^{2\beta}r^2}\{-2\rho_{,r}V_{ang}\overline{U}r^2-2(\bar{\eth}\rho)\overline{V}_{ang}e^{2\beta}J-4\rho_{,r}v_0r^2-2(\eth\rho)V_{ang}e^{2\beta}\overline{J}-2\rho_{,r}\overline{V}_{ang}Ur^2\\
&-2v_1(\bar{\eth}\rho)Ur^2+[2(\bar{\eth}\rho)V_{ang}e^{2\beta}+2(\eth\rho)\overline{V}_{ang}e^{2\beta}]K+4\rho_{,r}v_1V_wr^2-2v_1(\eth\rho)\overline{U}r^2\},
\end{aligned}
\tag{A3}
$$

$$
\begin{aligned}
F_a=&\frac{p_\rho}{4e^{2\beta}r^3}\{-2v_1\rho_{,r}\overline{V}_{ang}Ur^3-2v_1^2(\eth\rho)\overline{U}r^3-2v_1^2(\bar{\eth}\rho)Ur^3-4v_1\rho_{,r}v_0r^3+4v_1^2\rho_{,r}V_wr^3-2rv_1(\bar{\eth}\rho)\overline{V}_{ang}e^{2\beta}J\\
&-2rv_1(\eth\rho)V_{ang}e^{2\beta}\overline{J}+[2rv_1(\bar{\eth}\rho)V_{ang}e^{2\beta}+2rv_1(\eth\rho)\overline{V}_{ang}e^{2\beta}]K\\
&-2v_1\rho_{,r}V_{ang}\overline{U}r^3+4\rho_{,r}r^3e^{2\beta}\}\\
&+\frac{1}{4e^{2\beta}r^3}\{[-2r(\eth v_1)V_{ang}e^{2\beta}+2V_{ang}^2e^{2\beta}]\overline{J}+8\beta_{,r}v_1v_0r^3-2v_1U(\bar{\eth}v_1)r^3+2v_1^2r^3V_{w,r}\\
&-2v_{1,r}\overline{U}V_{ang}r^3+4\beta_{,r}v_1r^3\overline{U}V_{ang}-2v_1r^3\overline{U}_{,r}V_{ang}+4V_wv_{1,r}v_1r^3-2v_{1,r}U\overline{V}_{ang}r^3\\
&+KJr\overline{J}_{,r}V_{ang}\overline{V}_{ang}e^{2\beta}-2v_1\overline{U}(\eth v_1)r^3+4\beta_{,r}v_1r^3U\overline{V}_{ang}-4v_{1,r}v_0r^3-r\overline{J}_{,r}V_{ang}^2e^{2\beta}\\
&+[-4V_{ang}\overline{V}_{ang}e^{2\beta}+2r(\eth v_1)\overline{V}_{ang}e^{2\beta}+2r(\bar{\eth}v_1)V_{ang}e^{2\beta}]K-4V_w\beta_{,r}v_1^2r^3\\
&-2v_1r^3U_{,r}\overline{V}_{ang}+[-2r(\bar{\eth}v_1)\overline{V}_{ang}e^{2\beta}+2\overline{V}_{ang}^2e^{2\beta}]J-2J\overline{J}rK_{,r}V_{ang}\overline{V}_{ang}e^{2\beta}\\
&+K\overline{J}rJ_{,r}V_{ang}\overline{V}_{ang}e^{2\beta}-rJ_{,r}\overline{V}_{ang}^2e^{2\beta}\}.
\end{aligned}
\tag{A4}
$$

[1] N.T. Bishop, R. Gomez, L. Lehner, M. Maharaj, and J. Winicour, Phys. Rev. D **56**, 6298 (1997).

[2] L. Lehner, N.T. Bishop, R. Gomez, B. Szilagyi, and J. Winicour, Phys. Rev. D (to be published), gr-qc/9809034.

[3] J.A. Font, M. Miller, W.M. Suen, and M. Tobias, ''Three Dimensional Numerical General Relativistic Hydrodynamics I: Formulations, Methods and Code Tests,'' gr-qc/9811015.

[4] R. Gómez, L. Lehner, R. Marsa, and J. Winicour, Phys. Rev. D **57**, 4778 (1997).

[5] P. Papadopoulos and J. Font, ''Relativistic hydrodynamics on spacelike and null surfaces: Formalism and computation of spherically symmetric spacetimes,'' gr-qc/9902018.

[6] N.T. Bishop and P. Haines, Quaestiones Mathematicae **19**, 259 (1996).

[7] M.R. Dubal, R.A. d'Inverno, and J.A. Vickers, Phys. Rev. D **58**, 044019 (1998).

[8] R. Gomez, R. Marsa, and J. Winicour, Phys. Rev. D **56**, 631 (1997).

[9] T. Baumgarte, Astrophys. J. **443**, 717 (1995).

[10] N.T. Bishop, R. Gomez, L. Lehner, and J. Winicour, Phys. Rev. D **54**, 6153 (1996).

[11] N.T. Bishop, Class. Quantum Grav. **10**, 333 (1993).

[12] N.T. Bishop, C.J.S. Clarke, and R.A. d'Inverno, Class. Quantum Grav. **7**, L23 (1993).

[13] R.A. Isaacson, J.S. Welling, and J. Winicour, J. Math. Phys. **24**, 1824 (1983).
[14] H. Bondi, M.J.G. van der Burg, and A.W.K. Metzner, Proc. R. Soc. London **A269**, 21 (1962).
[15] R.K. Sachs, Proc. R. Soc. London **A270**, 103 (1962).
[16] R. Gómez, L. Lehner, P. Papadopoulos, and J. Winicour, Class. Quantum Grav. **14**, 977 (1997).
[17] S.W. Hawking and G.F.R. Ellis, *The Large Scale Structure of Spacetime* (Cambridge University Press, Cambridge, England, 1973), p. 70.
[18] H. Stephani, *General Relativity—An Introduction to the Theory of the Gravitational Field*, 2nd ed. (Cambridge University Press, Cambridge, England, 1990), p. 83.
[19] J.R. Wilson, Astrophys. J. **173**, 431 (1972).
[20] R.A. Isaacson, J.S. Welling, and J. Winicour, J. Math. Phys. **26**, 2859 (1985).
[21] P. Papadopoulos and J.A. Font, Phys. Rev. D **59**, 044014 (1999).